

The Proton- Ω correlation function in Au+Au collisions at $\sqrt{s_{NN}}=200$ GeV

J. Adam¹¹, L. Adamczyk¹, J. R. Adams³⁴, J. K. Adkins²⁴, G. Agakishiev²², M. M. Aggarwal³⁶, Z. Ahammed⁵⁶, N. N. Ajitanand⁴⁸, I. Alekseev^{2,30}, D. M. Anderson⁵⁰, R. Aoyama⁵³, A. Aparin²², D. Arkhipkin⁴, E. C. Aschenauer⁴, M. U. Ashraf⁵², F. Atetalla²³, A. Attri³⁶, G. S. Averichev²², X. Bai⁹, V. Bairathi³¹, K. Barish⁸, A. J. Bassill⁸, A. Behera⁴⁸, R. Bellwied¹⁷, A. Bhasin²¹, A. K. Bhati³⁶, J. Bielcik¹², J. Bielcikova³³, L. C. Bland⁴, I. G. Bordyuzhin², J. D. Brandenburg⁴¹, A. V. Brandin³⁰, D. Brown²⁷, J. Bryslawskyj⁸, I. Bunzarov²², J. Butterworth⁴¹, H. Caines⁵⁹, M. Calderón de la Barca Sánchez⁶, J. M. Campbell³⁴, D. Cebra⁶, I. Chakaberia^{23,45}, P. Chaloupka¹², Z. Chang⁴, F-H. Chang³², N. Chankova-Bunzarova²², A. Chatterjee⁵⁶, S. Chattopadhyay⁵⁶, J. H. Chen⁴⁶, X. Chen¹⁹, X. Chen⁴⁴, J. Cheng⁵², M. Cherney¹¹, W. Christie⁴, G. Contin²⁶, H. J. Crawford⁵, S. Das⁹, T. G. Dedovich²², I. M. Deppner¹⁶, A. A. Derevschikov³⁸, L. Didenko⁴, C. Dilks³⁷, X. Dong²⁶, J. L. Drachenberg²⁵, J. C. Dunlop⁴, L. G. Efimov²², N. Elsey⁵⁸, J. Engelage⁵, G. Eppley⁴¹, R. Esha⁷, S. Esumi⁵³, O. Evdokimov¹⁰, J. Ewigleben²⁷, O. Eyer⁴, R. Fatemi²⁴, S. Fazio⁴, P. Federic³³, P. Federicova¹², J. Fedorisin²², P. Filip²², E. Finch⁴⁷, Y. Fisyak⁴, C. E. Flores⁶, L. Fulek¹, C. A. Gagliardi⁵⁰, T. Galatyuk¹³, F. Geurts⁴¹, A. Gibson⁵⁵, D. Grosnick⁵⁵, D. S. Gunarathne⁴⁹, Y. Guo²³, A. Gupta²¹, W. Guryn⁴, A. I. Hamad²³, A. Hamed⁵⁰, A. Harlenderova¹², J. W. Harris⁵⁹, L. He³⁹, S. Heppelmann⁶, S. Heppelmann³⁷, N. Herrmann¹⁶, A. Hirsch³⁹, L. Holub¹², S. Horvat⁵⁹, B. Huang¹⁰, X. Huang⁵², S. L. Huang⁴⁸, T. Huang³², H. Z. Huang⁷, T. J. Humanic³⁴, P. Huo⁴⁸, G. Igo⁷, W. W. Jacobs¹⁸, A. Jentsch⁵¹, J. Jia^{4,48}, K. Jiang⁴⁴, S. Jowzaee⁵⁸, E. G. Judd⁵, S. Kabana²³, D. Kalinkin¹⁸, K. Kang⁵², D. Kapukchyan⁸, K. Kauder⁴, H. W. Ke⁴, D. Keane²³, A. Kechechyan²², D. P. Kikola⁵⁷, C. Kim⁸, T. A. Kinghorn⁶, I. Kisel¹⁴, A. Kisel⁵⁷, L. Kochenda³⁰, L. K. Kosarzewski⁵⁷, A. F. Kraishan⁴⁹, L. Kramarik¹², L. Krauth⁸, P. Kravtsov³⁰, K. Krueger³, N. Kulathunga¹⁷, S. Kumar³⁶, L. Kumar³⁶, R. Kunnawalkam Elayavalli⁵⁸, J. Kvapil¹², J. H. Kwasizur¹⁸, R. Lacey⁴⁸, J. M. Landgraf⁴, J. Lauret⁴, A. Lebedev⁴, R. Lednicky²², J. H. Lee⁴, Y. Li⁵², W. Li⁴⁶, C. Li⁴⁴, X. Li⁴⁴, Y. Liang²³, J. Lidrych¹², T. Lin⁵⁰, A. Lipiec⁵⁷, M. A. Lisa³⁴, H. Liu¹⁸, P. Liu⁴⁸, F. Liu⁹, Y. Liu⁵⁰, T. Ljubicic⁴, W. J. Llope⁵⁸, M. Lomnitz²⁶, R. S. Longacre⁴, S. Luo¹⁰, X. Luo⁹, L. Ma¹⁵, G. L. Ma⁴⁶, R. Ma⁴, Y. G. Ma⁴⁶, N. Magdy⁴⁸, R. Majka⁵⁹, D. Mallick³¹, S. Margetis²³, C. Markert⁵¹, H. S. Matis²⁶, O. Matonoha¹², D. Mayes⁸, J. A. Mazer⁴², K. Meehan⁶, J. C. Mei⁴⁵, N. G. Minaev³⁸, S. Mioduszewski⁵⁰, D. Mishra³¹, B. Mohanty³¹, M. M. Mondal²⁰, I. Mooney⁵⁸, D. A. Morozov³⁸, Md. Nasim⁷, J. D. Negrete⁸, J. M. Nelson⁵, D. B. Nemes⁵⁹, M. Nie⁴⁶, G. Nigmatkulov³⁰, T. Niida⁵⁸, L. V. Nogach³⁸, T. Nonaka⁹, S. B. Nurushev³⁸, G. Odyniec²⁶, A. Ogawa⁴, S. Oh⁵⁹, K. Oh⁴⁰, V. A. Okorokov³⁰, D. Olvitt Jr.⁴⁹, B. S. Page⁴, R. Pak⁴, Y. Panebratsev²², B. Pawlik³⁵, H. Pei⁹, C. Perkins⁵, J. Pluta⁵⁷, J. Porter²⁶, M. Posik⁴⁹, N. K. Pruthi³⁶, M. Przybycien¹, J. Putschke⁵⁸, A. Quintero⁴⁹, S. K. Radhakrishnan²⁶, S. Ramachandran²⁴, R. L. Ray⁵¹, R. Reed²⁷, H. G. Ritter²⁶, J. B. Roberts⁴¹, O. V. Rogachevskiy²², J. L. Romero⁶, L. Ruan⁴, J. Rusnak³³, O. Rusnakova¹², N. R. Sahoo⁵⁰, P. K. Sahu²⁰, S. Salur⁴², J. Sandweiss⁵⁹, J. Schambach⁵¹, A. M. Schmah²⁶, W. B. Schmidke⁴, N. Schmitz²⁸, B. R. Schweid⁴⁸, F. Seck¹³, J. Seger¹¹, M. Sergeeva⁷, R. Seto⁸, P. Seyboth²⁸, N. Shah^{46,a}, E. Shahaliev²², P. V. Shanmuganathan²⁷, M. Shao⁴⁴, W. Q. Shen⁴⁶, F. Shen⁴⁵, S. S. Shi⁹, Q. Y. Shou⁴⁶, E. P. Sichtermann²⁶, S. Siejka⁵⁷, R. Sikora¹, M. Simko³³, S. Singha²³, D. Smirnov⁴, N. Smirnov⁵⁹, W. Solyst¹⁸, P. Sorensen⁴, H. M. Spinka³, B. Srivastava³⁹, T. D. S. Stanislaus⁵⁵, D. J. Stewart⁵⁹, M. Strikhanov³⁰, B. Stringfellow³⁹, A. A. P. Suaide⁴³, T. Sugiura⁵³, M. Sumbera³³, B. Summa³⁷, X. Sun⁹, Y. Sun⁴⁴, X. M. Sun⁹, B. Surrow⁴⁹, D. N. Svirida², P. Szymanski⁵⁷, Z. Tang⁴⁴, A. H. Tang⁴, A. Taranenko³⁰, T. Tarnowsky²⁹, J. H. Thomas²⁶, A. R. Timmins¹⁷, D. Tlusty⁴¹, T. Todoroki⁴, M. Tokarev²², C. A. Tomkiel²⁷, S. Trentalange⁷, R. E. Tribble⁵⁰, P. Tribedy⁴, S. K. Tripathy²⁰, O. D. Tsai⁷, B. Tu⁹, T. Ullrich⁴, D. G. Underwood³, I. Upsal^{4,45}, G. Van Buren⁴, J. Vanek³³, A. N. Vasiliev³⁸, I. Vassiliev¹⁴, F. Videbæk⁴, S. Vokal²², S. A. Voloshin⁵⁸, A. Vossen¹⁸, F. Wang³⁹, G. Wang⁷, Y. Wang⁵², Y. Wang⁹, J. C. Webb⁴, L. Wen⁷, G. D. Westfall²⁹, H. Wieman²⁶, S. W. Wissink¹⁸, R. Witt⁵⁴, Y. Wu²³, Z. G. Xiao⁵², W. Xie³⁹, G. Xie¹⁰, Z. Xu⁴, J. Xu⁹, Y. F. Xu⁴⁶, N. Xu²⁶, Q. H. Xu⁴⁵, Y. Yang³², C. Yang⁴⁵, S. Yang⁴, Q. Yang⁴⁵, Z. Ye¹⁰, Z. Ye¹⁰, L. Yi⁴⁵, K. Yip⁴, I. -K. Yoo⁴⁰, N. Yu⁹, H. Zbroszczyk⁵⁷, W. Zha⁴⁴, Z. Zhang⁴⁶, J. Zhang¹⁹, L. Zhang⁹, J. Zhang²⁶, Y. Zhang⁴⁴, X. P. Zhang⁵², S. Zhang⁴⁶, S. Zhang⁴⁴, J. Zhao³⁹, C. Zhong⁴⁶, C. Zhou⁴⁶, L. Zhou⁴⁴, Z. Zhu⁴⁵, X. Zhu⁵², M. Zyzak¹⁴

¹AGH University of Science and Technology, FPACS, Cracow 30-059, Poland

²Alkhanov Institute for Theoretical and Experimental Physics, Moscow 117218, Russia

³Argonne National Laboratory, Argonne, Illinois 60439

⁴Brookhaven National Laboratory, Upton, New York 11973

⁵University of California, Berkeley, California 94720

⁶University of California, Davis, California 95616

⁷University of California, Los Angeles, California 90095

- ⁸ *University of California, Riverside, California 92521*
⁹ *Central China Normal University, Wuhan, Hubei 430079*
¹⁰ *University of Illinois at Chicago, Chicago, Illinois 60607*
¹¹ *Creighton University, Omaha, Nebraska 68178*
¹² *Czech Technical University in Prague, FNSPE, Prague 115 19, Czech Republic*
¹³ *Technische Universität Darmstadt, Darmstadt 64289, Germany*
¹⁴ *Frankfurt Institute for Advanced Studies FIAS, Frankfurt 60438, Germany*
¹⁵ *Fudan University, Shanghai, 200433*
¹⁶ *University of Heidelberg, Heidelberg 69120, Germany*
¹⁷ *University of Houston, Houston, Texas 77204*
¹⁸ *Indiana University, Bloomington, Indiana 47408*
¹⁹ *Institute of Modern Physics, Chinese Academy of Sciences, Lanzhou, Gansu 730000*
²⁰ *Institute of Physics, Bhubaneswar 751005, India*
²¹ *University of Jammu, Jammu 180001, India*
²² *Joint Institute for Nuclear Research, Dubna 141 980, Russia*
²³ *Kent State University, Kent, Ohio 44242*
²⁴ *University of Kentucky, Lexington, Kentucky 40506-0055*
²⁵ *Lamar University, Physics Department, Beaumont, Texas 77710*
²⁶ *Lawrence Berkeley National Laboratory, Berkeley, California 94720*
²⁷ *Lehigh University, Bethlehem, Pennsylvania 18015*
²⁸ *Max-Planck-Institut für Physik, Munich 80805, Germany*
²⁹ *Michigan State University, East Lansing, Michigan 48824*
³⁰ *National Research Nuclear University MEPhI, Moscow 115409, Russia*
³¹ *National Institute of Science Education and Research, HBNI, Jatni 752050, India*
³² *National Cheng Kung University, Tainan 70101*
³³ *Nuclear Physics Institute AS CR, Prague 250 68, Czech Republic*
³⁴ *Ohio State University, Columbus, Ohio 43210*
³⁵ *Institute of Nuclear Physics PAN, Cracow 31-342, Poland*
³⁶ *Panjab University, Chandigarh 160014, India*
³⁷ *Pennsylvania State University, University Park, Pennsylvania 16802*
³⁸ *Institute of High Energy Physics, Protvino 142281, Russia*
³⁹ *Purdue University, West Lafayette, Indiana 47907*
⁴⁰ *Pusan National University, Pusan 46241, Korea*
⁴¹ *Rice University, Houston, Texas 77251*
⁴² *Rutgers University, Piscataway, New Jersey 08854*
⁴³ *Universidade de Sao Paulo, Sao Paulo, Brazil 05314-970*
⁴⁴ *University of Science and Technology of China, Hefei, Anhui 230026*
⁴⁵ *Shandong University, Jinan, Shandong 250100*
⁴⁶ *Shanghai Institute of Applied Physics, Chinese Academy of Sciences, Shanghai 201800*
⁴⁷ *Southern Connecticut State University, New Haven, Connecticut 06515*
⁴⁸ *State University of New York, Stony Brook, New York 11794*
⁴⁹ *Temple University, Philadelphia, Pennsylvania 19122*
⁵⁰ *Texas A&M University, College Station, Texas 77843*
⁵¹ *University of Texas, Austin, Texas 78712*
⁵² *Tsinghua University, Beijing 100084*
⁵³ *University of Tsukuba, Tsukuba, Ibaraki 305-8571, Japan*
⁵⁴ *United States Naval Academy, Annapolis, Maryland 21402*
⁵⁵ *Valparaiso University, Valparaiso, Indiana 46383*
⁵⁶ *Variable Energy Cyclotron Centre, Kolkata 700064, India*
⁵⁷ *Warsaw University of Technology, Warsaw 00-661, Poland*
⁵⁸ *Wayne State University, Detroit, Michigan 48201*
⁵⁹ *Yale University, New Haven, Connecticut 06520 and*
^a *Department of Physics, Indian Institute of Technology Patna, Bihar 801106, India*

We present the first measurement of the proton- Ω correlation function in heavy-ion collisions for central (0-40%) and peripheral (40-80%) Au+Au collisions at $\sqrt{s_{NN}}=200$ GeV by the STAR experiment at the Relativistic Heavy-Ion Collider (RHIC). Predictions for the ratio of peripheral collisions to central collisions for the proton- Ω correlation function are sensitive to the presence of a nucleon- Ω bound state. These predictions are based on the proton- Ω interaction extracted from (2+1)-flavor lattice QCD calculations at the physical point. The measured ratio of proton- Ω correlation function from peripheral (small system) to central (large system) collisions is less than unity for relative momentum smaller than 40 MeV/c. Comparison of our measured correlation ratio with the theoretical calculation slightly favors a proton- Ω bound system with a binding energy of ~ 27 MeV.

INTRODUCTION

The study of nucleon-nucleon (NN), hyperon-nucleon (YN) and hyperon-hyperon (YY) interactions are of fundamental importance in understanding relativistic heavy-ion collisions [1, 2], modeling of neutron stars [3–6] and examining the existence of various exotic hadrons [7–9]. A significant amount of NN scattering data acquired over the years allows us to construct precise NN potential models [10?]. The availability of nominal YN scattering data and no scattering data for the multi-strange YY systems makes the task of constructing YN and YY potentials very challenging. With the development of sophisticated computational techniques, it has become possible to carry out first principle calculations based on lattice Quantum Chromodynamics (QCD) to provide constraints on some of the NN, YY and YN interactions [11–15]. Very often the experimental information on the bound states of strange baryons and nucleons (hypernuclei) is used to provide information on YN interactions [16–18]. However, this method becomes difficult to use because these measurements are contaminated by many-body effects, which makes it very difficult to extract $N\Xi$, $N\Omega$, $Y\Xi$ and $Y\Omega$ interactions.

High-energy heavy-ion collisions produce a sizable number of hyperons in each collision [19], which provides an excellent opportunity to study the NN, YN and YY interactions. Measurement of two-particle correlations at low relative momentum, also known as femtoscopy, have been used to study the space-time dynamics of the source created in heavy-ion collisions. In addition to this, the measurement of two-particle correlations at low relative momentum can also be used to measure final state interactions (FSI) between NN, YN and YY. This approach has been used by the STAR experiment at RHIC to extract the FSI for $\Lambda\Lambda$ [20] and antiproton-antiproton [21].

Recent study of (2+1)-flavor lattice QCD simulations for heavy quark masses shows that the nucleon- Ω interaction ($N\Omega$) is attractive at all distances [15]. Using this $N\Omega$ interaction, it is shown that the shape of the two particle correlation function at low relative momentum changes substantially with the strength of the $N\Omega$ attraction [22]. However, the presence of the Coulomb interaction in the proton- Ω channel makes it difficult to access the strong interaction directly from the measured two-particle correlation function. Therefore, a new measure, namely the ratio of the correlation functions between the peripheral (small) and central (large) collision systems is proposed in Ref [22]. This ratio provides direct access to strong interaction between proton and Ω , independent of the model used for the emission source.

The attractive nature of an $N\Omega$ interaction leads to the possible existence of the $N\Omega$ dibaryon with strangeness = -3, spin = 2, and isospin = 1/2, which was first proposed in [23]. Such an $N\Omega$ dibaryon is the most interesting candidate [23–27] after the H-dibaryon [7]. The Pauli exclusion principle does not apply among

quarks in the $N\Omega$ dibaryon and it is stable against strong decay [28, 29]. Several attempts have been made to estimate the binding energy of the $N\Omega$ state in different QCD motivated models [15, 30]. The $N\Omega$ dibaryon can be produced in high-energy heavy-ion collisions through the coalescence mechanism [31]. For an S-wave bound state of nucleon and Ω , the strong decays to octet-decuplet systems are prohibited by kinematics and those into octet-octet systems (e.g. $\Lambda\Xi$) are suppressed dynamically due to the D-wave nature [15]. This makes direct searches via the invariant mass method very challenging in heavy-ion collisions. The measurement of the proton- Ω correlation function for peripheral and central Au+Au collisions at $\sqrt{s_{NN}} = 200$ GeV, presented in this Letter, will provide insight into the existence of an $N\Omega$ dibaryon.

DATA ANALYSIS

STAR is a large acceptance detector at RHIC [32]. The measurements presented in this Letter are from the data taken for Au+Au collisions at $\sqrt{s_{NN}} = 200$ GeV in 2011 and 2014. 5.30×10^8 minimum bias events from 2011 and 8.76×10^8 minimum bias events from 2014 were analyzed. The tracking and particle identification for the measurements were provided by the Time Projection Chamber (TPC) [33] and Time-of-Flight (TOF) [34] detectors. These detectors are located in a 0.5 T magnetic field, which allows determination of the momentum and charge of the particles traversing the TPC. Minimum bias triggered events were selected by requiring coincident signals at forward and backward rapidities in the Vertex Position Detectors (VPD) [35] and requiring a signal at mid-rapidity in the TOF. Centrality was determined by the charged particle multiplicity at mid-rapidity ($|\eta| < 0.5$) in the TPC. To suppress events from collisions with the beam pipe, the reconstructed primary vertex was required to lie within a 2 cm radial distance from the center of the beam pipe. In addition, the z -position of the vertex was required to lie within ± 40 and ± 6 cm of the center of the detector for the data from years 2011 and 2014, respectively.

Ω IDENTIFICATION

The TPC was used for tracking, decay topology and identification of particles for Ω ($\bar{\Omega}$) reconstruction in the pseudorapidity range $|\eta| < 1$. To reconstruct the Ω ($\bar{\Omega}$), the decay channel $\Omega(\bar{\Omega}) \rightarrow \Lambda K^-(\bar{\Lambda} K^+)$, with a branching ratio of 67.8%, with subsequent decay $\Lambda(\bar{\Lambda}) \rightarrow p\pi^-(\bar{p}\pi^+)$ (branching ratio of 63.9%) was used [36]. The Λ ($\bar{\Lambda}$) candidates were formed from pairs of p (\bar{p}) and π^- (π^+) tracks whose trajectories pointed to a common secondary decay vertex, which was well separated from the Ω ($\bar{\Omega}$) vertex. These Λ ($\bar{\Lambda}$) candidates were then combined with bachelor K^- (K^+) tracks, which points to a

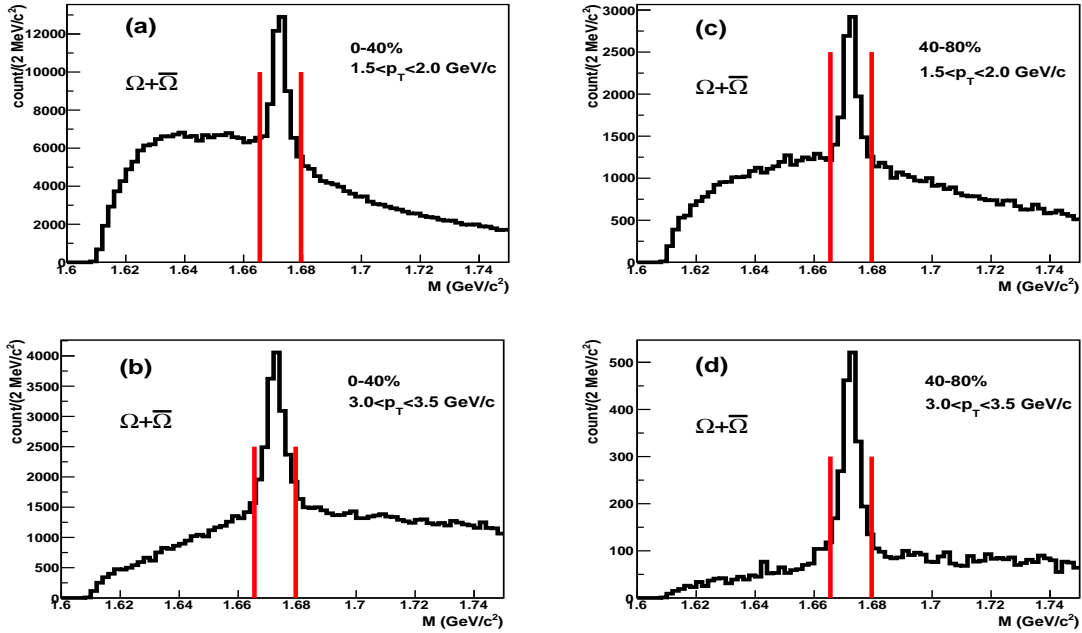


FIG. 1. (color online). Reconstructed invariant mass (M) distributions of combined Ω and $\bar{\Omega}$ sample for 0-40% Au+Au collisions at $\sqrt{s_{NN}}=200$ GeV for the transverse momentum (p_T) range $1.5 < p_T < 2.0$ GeV/ c (a) and $3.0 < p_T < 3.5$ GeV/ c (b). The invariant mass distributions of combined Ω and $\bar{\Omega}$ sample for 40-80% Au+Au collisions at $\sqrt{s_{NN}}=200$ GeV for the transverse momentum (p_T) range $1.5 < p_T < 2.0$ GeV/ c (c) and $3.0 < p_T < 3.5$ GeV/ c (d). The solid lines at 1.665 and 1.679 GeV/ c^2 show the mass region of the reconstructed Ω and $\bar{\Omega}$ candidates used for the measurement of the proton- Ω correlation function.

common decay vertex well separated from the primary vertex. The decay length (DL) of an Ω ($\bar{\Omega}$) candidate was required to be larger than 4 cm from the primary vertex. As listed in Table I, additional selection criteria on the distance of closest approach (DCA) between the two Λ ($\bar{\Lambda}$) daughter tracks, between the Λ ($\bar{\Lambda}$) and bachelor track, the Λ ($\bar{\Lambda}$) and the primary vertex position were applied to select Ω ($\bar{\Omega}$). Furthermore, the pointing angle of Ω ($\bar{\Omega}$) track with respect to the primary vertex ($|(\mathbf{r}_\Omega - \mathbf{r}_{PV}) \times \mathbf{p}_\Omega|/|\mathbf{r}_\Omega - \mathbf{r}_{PV}||\mathbf{p}_\Omega|$, where \mathbf{r} is the position of Ω and primary vertex, respectively and \mathbf{p}_Ω is the momentum of Ω) were applied to select Ω ($\bar{\Omega}$). To reduce the combinatorial background, Λ ($\bar{\Lambda}$) candidates were selected in the invariant mass range between 1.112 and 1.120 GeV/ c^2 . In addition, the candidates due to misidentification of π^- (π^+) tracks as the bachelor K^- (K^+) tracks were removed by checking a Ξ hypothesis. The invariant mass distributions of combined Ω and $\bar{\Omega}$ candidates for 0-40% and 40-80% Au+Au collisions at $\sqrt{s_{NN}}=200$ GeV for the transverse momentum (p_T) ranges $1.5 < p_T < 2.0$ GeV/ c and $3.0 < p_T < 3.5$ GeV/ c are shown in Figure 1(a-d). The signal (S) to signal+background ($S+B$) ratio, integrated over $\pm 3\sigma$, is 0.2 for the p_T range $1.5 < p_T < 2.0$ GeV/ c and 0.4 for the p_T range $3.0 < p_T < 3.5$ GeV/ c in 0-40% centrality and is 0.3 for the p_T range $1.5 < p_T < 2.0$ GeV/ c and 0.7 for the p_T range $3.0 < p_T < 3.5$ GeV/ c in 40-80% centrality. All

candidates with invariant mass between 1.665 and 1.679 GeV/ c^2 were used in the analysis.

PROTON IDENTIFICATION

The TOF and TPC detectors were used for proton (antiproton) identification in the pseudorapidity range $|\eta| < 1$. The proton tracks were selected if their DCA was less than 0.5 cm to the primary vertex, greater than 20 points were measured out of a maximum of 45, and the number of points used in track reconstruction divided by the number of possible points was greater than 0.52 in order to prevent split tracks. The time of flight of the particles reaching the TOF detector along with the tracking information from the TPC detector was used to calculate the square of the particle mass (m^2) to identify protons. Figure 2 shows m^2 from the TOF detector versus momentum from the TPC. All candidates with m^2 between 0.75 and 1.10 (GeV/ c^2) 2 were used in the analysis.

TWO-PARTICLE CORRELATION FUNCTION

The two-particle correlation function is defined as:

Selection criteria	0-40%		40-80%
	$p_T < 2.5$ GeV/c	$p_T > 2.5$ GeV/c	All p_T
Ω DCA	< 0.6 cm	< 0.7 cm	< 0.8 cm
Λ DCA	> 0.4 cm	> 0.3 cm	> 0.3 cm
DL(Ω)	> 4.0 cm	> 4.0 cm	> 4.0 cm
DL(Λ)	> 6.0 cm	> 6.0 cm	> 5.0 cm
$ (r_\Omega - r_{PV}) \times p_\Omega / r_\Omega - r_{PV} p_\Omega $	< 0.05	< 0.08	< 0.15
$DL(\Omega) < DL(\Lambda)$	Yes	Yes	Yes
proton DCA	> 0.8 cm	> 0.8 cm	> 0.6 cm
pion DCA	> 2.0 cm	> 2.0 cm	> 1.8 cm
bachelor DCA	> 1.2 cm	> 1.2 cm	> 1.0 cm
proton to pion DCA	< 0.8 cm	< 0.8 cm	< 1.0 cm
Λ DCA to bachelor	< 0.8cm	< 0.8cm	< 1.0cm
$ M_\Lambda - 1.1156 $ GeV/ c^2	< 0.007 GeV/ c^2	< 0.007 GeV/ c^2	< 0.007 GeV/ c^2
$ M_\Omega - 1.672 $ GeV/ c^2	< 0.007 GeV/ c^2	< 0.007 GeV/ c^2	< 0.007 GeV/ c^2

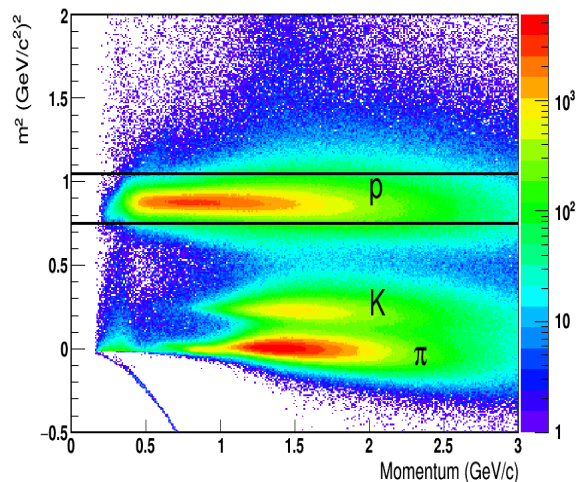
TABLE I. Selection criteria for Ω and $\bar{\Omega}$ reconstruction.

FIG. 2. (color online) Proton identification using the time of flight and momentum from the TOF and the TPC detectors, respectively. The solid lines show lower and upper cuts to select protons.

$$C_{\text{measured}}(k^*) = \frac{A(k^*)}{B(k^*)}, \quad (1)$$

where $A(k^*)$ is the distribution of the invariant relative momentum, where $k^* = |k^*|$ is relative momentum of one of the particles in the pair rest frame, for a proton and Ω pair or anti-proton and $\bar{\Omega}$ pair from the same event. $B(k^*)$ is the reference distribution generated by mixing particles from different events with the same centrality and with approximately the same vertex position along the z -direction. The same single- and pair-particle cuts were applied for real and mixed events. The data analysis

was done in nine centrality bins: 0-5%, 5-10%, 10-20%, 20-30%, 30-40%, 40-50%, 50-60%, 60-70% and 70-80% for both same events and mixed events. The final results were combined and presented in two centrality bins: 0-40% and 40-80%. The efficiency and acceptance effects canceled out in the ratio $A(k^*)/B(k^*)$. Corrections to the raw correlation functions were applied according to the expression:

$$C'(k^*) = \frac{C_{\text{measured}}(k^*) - 1}{P(k^*)} + 1, \quad (2)$$

where the pair purity, $P(k^*)$, was calculated as a product of $S/(S+B)$ for the Ω ($\bar{\Omega}$) and purity of the proton (antiproton). The selected sample of proton candidates also included secondary protons from Λ , Σ and Ξ decays. The estimated fraction of primary protons (antiprotons) from thermal model [37] studies is 52% (48%) [38]. The purity of the proton sample is obtained as a product of identification probability and fraction of primary protons. The pair purity is 0.2 (0.36) for 0-40% (40-80)% centrality and is constant over the analyzed range of invariant relative momentum.

The effect of momentum resolution on the correlation functions has also been investigated using simulated tracks from Ω decay and tracks for protons, with known momenta, embedded into real events. Correlation functions have been corrected for momentum resolution using the expression:

$$C(k^*) = \frac{C'(k^*)C_{\text{in}}(k^*)}{C_{\text{res}}(k^*)}, \quad (3)$$

where $C(k^*)$ represents the corrected correlation function, and $C_{\text{in}}(k^*)/C_{\text{res}}(k^*)$ is the correction factor. $C_{\text{in}}(k^*)$ was calculated without taking into account the effect of momentum resolution and $C_{\text{res}}(k^*)$ included the effect of momentum resolution applied to each Ω and proton candidates. More details related to these corrections

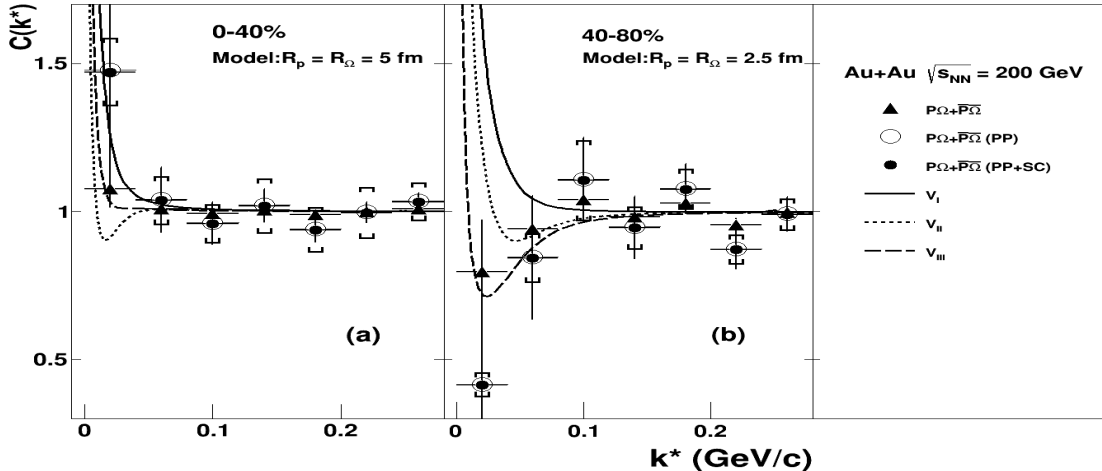


FIG. 3. Measured correlation function ($C(k^*)$) for proton- Ω and antiproton- $\bar{\Omega}$ ($P\Omega + \bar{P}\bar{\Omega}$) for (0-40)% (a) and (40-80)% (b) Au+Au collisions at $\sqrt{s_{NN}} = 200$ GeV. The triangles represent raw correlations, open circles represent pair-purity corrected (PP) correlations, and solid circles represent pair-purity and smearing corrected (PP+SC) correlations. The error bars correspond to statistical errors and caps correspond to the systematic errors. The predictions from [22] for proton- Ω interaction potentials V_I , V_{II} and V_{III} for source sizes $R_p = R_\Omega = 5$ fm and $R_p = R_\Omega = 2.5$ fm are shown in (a) and (b) respectively.

can be found in Ref. [39]. The impact of momentum resolution on correlation functions is negligible compared with statistical errors.

To study the shape of correlation function for the background, the candidates from the side-bands of invariant mass of Ω are chosen in the range $M < 1.665$ GeV/ c^2 and $M > 1.679$ GeV/ c^2 . These selected candidates are then combined with the proton tracks from the same event to construct the relative momentum for the same event. The relative momentum for the mixed event is generated by combining the selected candidates from the side-band of invariant mass of Ω with protons from different events with approximately the same vertex position along the z -direction.

RESULTS AND DISCUSSION

After applying the selection criteria for proton and Ω identification, as mentioned in the data analysis section, a total of 38065 ± 195 (8816 ± 94) and 3037 ± 55 (679 ± 26) pairs of proton- Ω and antiproton- $\bar{\Omega}$ for $k^* < 0.2$ (0.1) GeV/ c are observed for (0-40)% and (40-80)% Au+Au collisions, respectively. The measured proton- Ω and antiproton- $\bar{\Omega}$ correlation functions, $P\Omega + \bar{P}\bar{\Omega}$, the correlation functions after corrections for pair purity, $P\Omega + \bar{P}\bar{\Omega}$ (PP), and the correlation function after corrections for pair purity and momentum smearing, $P\Omega + \bar{P}\bar{\Omega}$ (PP+SC), for 0-40% and 40-80% Au+Au collisions at $\sqrt{s_{NN}} = 200$ GeV are shown in Figures 3 (a) and 3 (b). The systematic errors for the measured proton- Ω corre-

lation function were estimated by varying the following requirements for the selection of Ω candidates: the decay length, DCA of Ω to the primary vertex, pointing angle cuts and mass range, which affect the purity of the Ω sample. The DCA and m^2 requirements were varied to estimate systematic from the proton purity. In addition, systematic errors from normalization and feed-down contributions were also estimated. The systematic errors from different sources were then added in quadrature. The combined systematic errors are shown in Figure 3 as caps for each bin of the correlation function.

Predictions for the proton- Ω correlation function from [22] for proton- Ω interaction potentials V_I , V_{II} and V_{III} for a static source with sizes $R_p = R_\Omega = 5.0$ fm and $R_p = R_\Omega = 2.5$ fm are also shown in the Figure 3(a) and Figure 3(b). The selected source sizes are not fit to the experimental data. The choice of the potentials in Ref. [22] is based on an attractive $N\Omega$ interaction in the 5S_2 channel from the lattice QCD simulations with heavy u -, d -, s - quarks from Ref. [15]. The potential V_{II} is obtained by fitting the lattice QCD data with a function $V(r) = b_1 e^{-b_2 r^2} + b_3 (1 - e^{-b_4 r^2}) (e^{-b_5 r}/r)^2$, where b_1 and b_3 are negative and b_2 , b_4 and b_5 are positive, which represents a case with shallow $N\Omega$ bound state. Two more potentials V_I and V_{III} represent cases without a $N\Omega$ bound state and a deep $N\Omega$ bound state, respectively. Binding energy (E_b), scattering length (a_0) and effective range (r_{eff}) for the $N\Omega$ interaction potentials V_I , V_{II} and V_{III} are listed in Table II [22]. The measured correlation functions for $P\Omega + \bar{P}\bar{\Omega}$ are in agreement with the predicted trend for the $P\Omega$ correlation functions with inter-

action potentials V_I , V_{II} and V_{III} for the 0-40% Au+Au collisions as shown in Figure 3(a). However, due to limited statistics at lower k^* , strong enhancement due to Coulomb interaction is not visible in the 40-80% Au+Au collisions in Figure 3(b).

Spin-2 p Ω potentials	V_I	V_{II}	V_{III}
\mathbf{E}_b (MeV)	-	6.3	26.9
\mathbf{a}_0 (fm)	-1.12	5.79	1.29
\mathbf{r}_{eff} (fm)	1.16	0.96	0.65

TABLE II. Binding energy (\mathbf{E}_b), scattering length (\mathbf{a}_0) and effective range (\mathbf{r}_{eff}) for the Spin-2 proton- Ω potentials [22].

The measured proton- Ω and antiproton- $\bar{\Omega}$ correlation function includes three effects coming from the elastic scattering in the 5S_2 channel, the strong absorption in the 3S_1 channel and the long-range Coulomb interactions. The Coulomb interaction between the positively charged proton and negatively charged Ω introduces a strong enhancement in the correlation function at small k^* , as seen in Figure 3. One can remove the Coulomb enhancement using a Gamow correction, however, this simple correction is not good enough to extract the characteristic feature of correlation function from strong interaction. A full correction with source-size dependence is needed to isolate the effect of strong interaction from Coulomb enhancement. Therefore the ratio of correlation function between small and large collision systems, is proposed in [22] as a model-independent way to access the strong interaction with less contamination from the Coulomb interaction.

The ratio of combined proton- Ω and antiproton- $\bar{\Omega}$ correlation function from peripheral (40-80%) to central (0-40%) collisions, defined as $R = C_{40-80}/C_{0-40}$, for proton- Ω and antiproton- $\bar{\Omega}$ ($P\Omega + \bar{P}\bar{\Omega}$) is shown in Figure 4. The systematic uncertainties are propagated from the measured correlation functions for 0-40% and 40-80% centrality and are shown as caps. For the background study, the candidates from the side-bands of Ω invariant mass were combined with protons to construct the correlation function. The same ratio, R , for the background is unity and is shown as open crosses in Figure 4. Previous measurements of source size for π - π , K_S^0 - K_S^0 , proton-proton and proton- Λ correlations show that the source size decreases as the transverse mass increases [21, 38-41]. Using this transverse mass dependence [41], the expected source size for proton- Ω is 2-3 fm for peripheral collisions and 3-5 fm for central collisions. The predictions for the ratio of small system to large system from Refs. [22, 42] for proton- Ω interaction potentials V_I , V_{II} and V_{III} for static source with different source sizes (S,L) = (2,3), (2,4), (2.5, 5) and (3,5) fm, where S and L correspond to small and large collision system, are shown in Figure 4(a-d). A small variation in the source size does not change the characteristic of the ratio for the choice of three potentials.

Predictions for the ratio of small to large system with the effects of collective expansion are also shown in the Figure 4(e) [22]. The transverse source sizes are taken as $R_p^{tr} = R_\Omega^{tr} = 2.5$ fm for small system and $R_p^{tr} = R_\Omega^{tr} = 5$ fm for large system. The temperature at the thermal freeze-out is $T_{p,\Omega} = 164$ MeV for peripheral collisions and $T_{p,\Omega} = 120$ MeV for the central collisions [43, 44] and the proper-time at the thermal freeze-out is $\tau_p(\tau_\Omega) = 3(2)$ fm/c for the peripheral collisions and $\tau_p(\tau_\Omega) = 20(10)$ fm/c for the central collisions [45].

The predictions with expanding source for the proton- Ω interaction potentials V_I and V_{II} are 3σ larger than the data at $k^* = 20$ MeV/c. The prediction for the proton- Ω interaction potential V_{III} with expanding source and static source are within 1σ of the data at $k^* = 20$ MeV/c. As shown in Figure 4, the measured ratios at $k^* = 20$ and 60 MeV/c are $R = 0.28 \pm 0.35_{stat} \pm 0.03_{sys}$ (background = $0.96 \pm 0.13_{stat}$) and $R = 0.81 \pm 0.22_{stat} \pm 0.08_{sys}$ (background = $0.97 \pm 0.05_{stat}$), respectively. Comparing these values with the model calculations shown in Figure 5(b) of the Ref. [22], where a bound state with $\mathbf{E}_b \sim 27$ MeV for the proton- Ω system is assumed in calculation, we conclude that our data favor a positive scattering length for the proton- Ω interactions. The positive scattering length and the measured ratio of proton- Ω correlation function from peripheral to central collisions less than unity for $k^* < 40$ MeV/c favors the proton- Ω interaction potential V_{III} with $\mathbf{E}_b \sim 27$ MeV for proton and Ω .

CONCLUSIONS

The first measurement of the proton- Ω correlation function in heavy-ion collisions for Au+Au collisions at $\sqrt{s_{NN}} = 200$ GeV is presented in this Letter. The measured ratio of proton- Ω correlation function from peripheral to central collisions is compared with the predictions based on proton- Ω interaction extracted from (2+1)-flavor lattice QCD simulations. At present, due to limited statistics, it is not possible to extract the interaction parameters. However the measured ratio of proton- Ω correlation function from peripheral to central collisions less than unity for $k^* < 40$ MeV/c within 1σ indicates that the scattering length is positive for the proton- Ω interaction and favors the proton- Ω bound state hypothesis.

ACKNOWLEDGMENTS

We thank Dr. Kenji Morita, Dr. Akira Ohnishi, Dr. Faisal Etminan and Dr. Tetsuo Hatsuda for providing the calculation and enlightening discussions. We thank the RHIC Operations Group and RCF at BNL, the NERSC Center at LBNL, and the Open Science Grid consortium for providing resources and support. This work was supported in part by the Office of Nuclear Physics within the

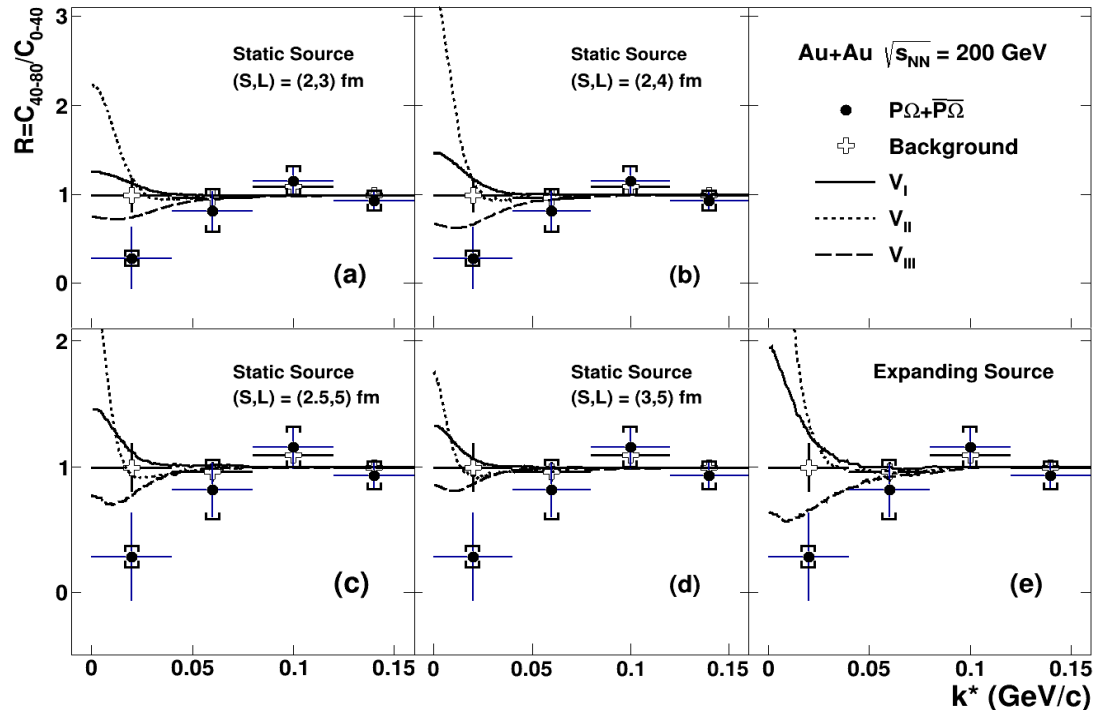


FIG. 4. The solid circle represents the ratio (R) of small system (40-80% collisions) to large system (0-40% collisions) for proton- Ω and antiproton- $\bar{\Omega}$ ($P\Omega + \bar{P}\bar{\Omega}$). The error bars correspond to the statistical errors and caps correspond to systematic errors. The open crosses represent the ratio for background candidates from the side-band of Ω invariant mass. Predictions for the ratio of small system to large system [22, 42] for proton- Ω interaction potentials V_I , V_{II} and V_{III} for static source with different source sizes $(S,L) = (2,3)$, $(2,4)$, $(2.5, 5)$ and $(3,5)$ fm, where S and L corresponding to small and large systems, are shown in (a), (b), (c) and (d) respectively. In addition, the prediction for the expanding source is shown in (e).

U.S. DOE Office of Science, the U.S. National Science Foundation, the Ministry of Education and Science of the Russian Federation, National Natural Science Foundation of China, Chinese Academy of Science, the Ministry of Science and Technology of China (973 Program No. 2014CB845400, 2015CB856900) and the Chinese Ministry of Education, the National Research Foundation of Korea, Czech Science Foundation and Ministry of Education, Youth and Sports of the Czech Republic, Department of Atomic Energy and Department of Science and Technology of the Government of India, the National Science Centre of Poland, the Ministry of Science, Education and Sports of the Republic of Croatia, RosAtom of Russia and German Bundesministerium für Bildung, Wissenschaft, Forschung und Technologie (BMBF) and the Helmholtz Association.

[1] A. R. Bodmer, Phys. Rev. D **4**, 1601 (1971).
 [2] E. Witten, Phys. Rev. D **30**, 272 (1984).
 [3] M. Prakash and J. M. Lattimer, Nucl. Phys. A **639**, 433c (1998).
 [4] H. J. Schulze, A. Polls, A. Ramos and I. Vidana, Phys.

Rev. C **73**, 058801 (2006).
 [5] S. Weissenborn, D. Chatterjee and J. Schaffner-Bielich, Nucl. Phys. A **881**, 62 (2012).
 [6] S. Petschauer, J. Haidenbauer, N. Kaiser, U.-G. Maißner and W. Weise, Eur. Phys. J. A **52**, 15 (2016).
 [7] R. Jaffe, Phys. Rev. Lett. **38**, 195 (1977).
 [8] V. G. J. Stoks and T. A. Rijken, Phys. Rev. C **59**, 3009 (1999).
 [9] Z. Y. Zhang, Y. W. Yu, C. R. Ching, T. H. Ho, and Z. D. Lu, Phys. Rev. C **61**, 065204 (2000).
 [10] R. Machleidt, I. Slaus, J. Phys. G **27**, R69 (2001).
 [11] T. Inoue *et al.* (HAL QCD Collaboration), Prog. Theor. Phys. **124**, 591 (2010).
 [12] S. R. Beane *et al.* (NPLQCD Collaboration), Phys. Rev. Lett. **106**, 162001 (2011).
 [13] T. Inoue *et al.* (HAL QCD Collaboration), Phys. Rev. Lett. **106**, 162002 (2011).
 [14] T. Inoue *et al.* (HAL QCD Collaboration), Nucl. Phys. A **881**, 28 (2012).
 [15] F. Etminan *et al.* (HAL QCD Collaboration), Nucl. Phys. A **928**, 89 (2014).
 [16] B. I. Abelev *et al.* (STAR Collaboration), Science **328**, 58 (2010).
 [17] L. Adamczyk *et al.* (STAR Collaboration), Phys. Rev. C **97**, 054909 (2018).
 [18] A. Gal, E. V. Hungerford and D. J. Millener, Rev. Mod. Phys. **88**, 035004 (2016) and references therein.
 [19] J. Adams *et al.* (STAR Collaboration), Phys. Rev. Lett.

- 98**, 062301 (2007).
- [20] L. Adamczyk *et al.* (STAR Collaboration), Phys. Rev. Lett. **114**, 022301 (2015).
- [21] L. Adamczyk *et al.* (STAR Collaboration), Nature **527**, 345 (2015).
- [22] K. Morita, A. Ohnishi, F. Etminan and T. Hatsuda, Phys. Rev. C **94**, 031901 (R) (2016).
- [23] T. Goldman, K. Maltman, G.J. Stephenson, K.E. Schmidt and F. Wang, Phys. Rev. Lett. **59**, 627 (1987).
- [24] B. Schwesinger, F.G. Scholtz and H.B. Geyer, Phys. Rev. D **51**, 1228 (1995).
- [25] M. Oka, Phys. Rev. D **38**, 298 (1988).
- [26] H. Pang, J. Ping, F. Wang, T. Goldman and E. Zhao, Phys. Rev. C **69**, 065207 (2004).
- [27] H. Pang, J. Ping, L. Chen, F. Wang and T. Goldman, Phys. Rev. C **70**, 035201 (2004).
- [28] M. Chen, H. Huang, J. Ping and F. Wang, Phys. Rev. C **83**, 015202 (2011).
- [29] H. Huang, J. Ping and F. Wang, Phys. Rev. C **92**, 065202 (2015).
- [30] Q. B. Li and P. N. Shen, Eur. Phys. J. A **8**, 417 (2000).
- [31] N. Shah, Y. G. Ma, J. H. Chen and S. Zhang, Phys. Lett. B **754**, 6 (2016).
- [32] K. H. Ackermann *et al.* (STAR Collaboration), Nucl. Instrum. and Meth. A **499**, 624 (2003).
- [33] M. Anderson *et al.*, Nucl. Instrum. and Meth. A **499**, 659 (2003).
- [34] W. J. Llope (STAR Collaboration), Nucl. Instrum. and Meth. A **661**, S110 (2012).
- [35] W. J. Llope *et al.*, Nucl. Instrum. and Meth. A **759**, 23 (2014).
- [36] C. Patrignani *et al.* (Particle Data Group), Chin. Phys. C **40**, 100001 (2016).
- [37] M. Chojnacki, A. Kisiel, W. Florkowski, W. Broniowski, Comput. Phys. Commun. **183**, 746 (2012).
- [38] J. Adams *et al.* (STAR Collaboration), Phys. Rev. C **74**, 064906 (2006).
- [39] J. Adams *et al.* (STAR Collaboration), Phys. Rev. C **71**, 044906 (2005).
- [40] B. I. Abelev *et al.* (STAR Collaboration), Phys. Rev. C **74**, 054902 (2006).
- [41] H. Zbroszczyk, Studies of Baryon-Baryon Correlations in Relativistic Nuclear Collisions Registered at the STAR Experiment, Ph. D. Thesis, https://drupal.star.bnl.gov/STAR/files/Zbroszczyk_Hanna.pdf.
- [42] Private communications with Kenji Morita, Akira Ohnishi, Faisal Etminan and Tetsuo Hatsuda.
- [43] B. Abelev *et al.* (ALICE Collaboration), Phys. Lett. B **728**, 216 (2014), Erratum: Phys. Lett. B **734**, 409 (2014).
- [44] C. Shen, U. Heinz, P. Huovinen and H. Song, Phys. Rev. C **84**, 044903 (2011).
- [45] X. Zhu, F. Meng, H. Song and Y. X. Liu, Phys. Rev. C **91**, 034904 (2015).